

ACCELERATION SCHEDULES FOR A RECIRCULATING HEAVY-ION ACCELERATOR*

W. M. Sharp and D. P. Grote, LLNL, Livermore, CA

Abstract

The recent development of miniature inductive adders has made it feasible to design programmable high-repetition-rate pulsers with a substantially higher voltage than is possible using a conventional field-effect transistor architecture. Prototype pulsers using the new technology are being developed as part of a series experiments at Lawrence Livermore National Laboratory (LLNL) to test the concept of a recirculating induction accelerator. Preliminary numerical work is reported here to determine what effects the higher-voltage pulsers would have on the beam quality of the LLNL small recirculator.

1 INTRODUCTION

A series of scaled experiments is underway at the Lawrence Livermore National Laboratory (LLNL) to test the concept of a recirculating induction accelerator or ‘‘recirculator.’’ The pulsed-power circuitry used to drive the induction modules on this ‘‘small recirculator’’ attains the needed precision and repetition rate by using a parallel array of field-effect transistors (FETs), which currently have a voltage limit of about 500V. Due to this limit, the original design required an induction modules or ‘‘cells’’ in each available half-lattice period (HLP) to meet the goal of doubling the beam velocity over fifteen laps. The pulsers for these modules constitute about half of the projected hardware cost of the small recirculator.

Recently, a project has been carried out jointly by the LLNL heavy-ion fusion group and First Point Scientific, Inc. (FPSI) to design prototype high-voltage pulsers for the small recirculator using the miniature inductive adders developed by FPSI. If successful, the new pulsers might lower the cost of the small recirculator by substantially reducing the number of acceleration modules.

The possible use of higher-voltage pulsers raises the question of whether applying stronger but less-frequent acceleration and control fields will seriously degrade beam quality in the LLNL small recirculator. In this paper, we report preliminary numerical work to compare the effects of using between five and thirty-four pulsers, using several acceleration schedules for each configuration.

2 METHOD

Acceleration schedules are examined here with the fast-running beam-dynamics code CIRCE [1], which combines an envelope description of transverse dynamics with a fluid-like treatment of longitudinal dynamics. For each acceleration schedule, the electric potential $V(t)$ across

induction modules is set up by a two-step calculation. A modified version of an approach developed by Kim and Smith [2] is used to generate acceleration fields for self-similar compression in the absence of the longitudinal space-charge field. Longitudinal-control fields or ‘‘ears’’ are then added to balance the longitudinal force due to the beam space charge.

As originally formulated, the Kim-Smith approach assumes that beam slices have ballistic trajectories between induction cells, so the velocity between the n th cell, centered at longitudinal position s_n , and the next one at s_{n+1} is

$$\beta_{n+1}^i c = \frac{s_{n+1} - s_n}{t_{n+1}^i - t_n^i} \equiv \frac{\delta s_n}{\delta t_n^i}, \quad (1)$$

where the slice arrival times t_{n+1}^i are chosen so that the beam current I_b at s_{n+1} is self-similar to that at s_n . When that the cell length is negligible, the voltage V_n^i needed in the n th cell at time t_n^i is then given approximately by

$$V_n^i \approx \frac{\bar{\gamma}_i^3 M c^2}{2q e} [(\beta_{n+1}^i)^2 - (\beta_n^i)^2], \quad (2)$$

where q and M are the charge state and mass of beam ions, and $\bar{\gamma}_i$ is the Lorentz factor associated with $\bar{\beta}_i \equiv \frac{1}{2}(\beta_n^i + \beta_{n+1}^i)$.

The velocity estimate in Eq. (1) is suitable for a beam in a straight lattice, in which the design orbit coincides with the beam-pipe axis. In a circular accelerator like a recirculator, however, the head-to-tail velocity variation or ‘‘velocity tilt’’ needed for beam compression causes the lower-energy beam head to have a trajectory inside the design orbit, and the higher-energy tail has a trajectory outside it. This centroid displacement alters the path length of a slice in a bend and must be accounted for Eq. (1). A simple calculation using the approximation of continuous focusing shows that, for electric sector bends, each with an occupancy η_b , a radius ρ , and a mean radius $\bar{\rho} \equiv \rho/\eta_b$, the beam displacement \bar{X} in the accelerator plane, averaged over the alternating-gradient flutter motion, is

$$\bar{X} \approx \frac{1}{\frac{\sigma_0^2}{4L^2} - \frac{K}{R^2} + \frac{2}{\bar{\rho}}} \frac{2}{\bar{\rho}} \frac{\Delta p}{p}. \quad (3)$$

Here, R is the beam-pipe radius, L is the half-lattice period, and σ_0 is the betatron phase advance over a full lattice period $2L$ in the absence of space charge. The ‘‘momentum error’’ $\Delta p \equiv p - p_0$ is difference between the local beam momentum $p \equiv \gamma\beta M c$ and the design momentum $p_0 = [q e \gamma M E_{bx} \rho]^{1/2}$, which is the value for which an ion will stay on the design orbit in a sector bend with a radius ρ and field strength E_{bx} . For a magnetic sector bend with a field strength B_{by} , the design momentum becomes $p_0 = q e \gamma M B_{by} \rho$, but the \bar{X} expression corresponding to Eq. (3) differs only in the factor $2/\bar{\rho}$ being replaced by $1/\bar{\rho}$. The phase-advance depression caused by

* Work performed under the auspices of the U. S. Department of Energy by Lawrence Livermore National Laboratory under Contract No. W-7405-ENG-48.

the beam space charge is accounted for by the term proportional to the perveance $K \equiv 2qeI_b/[4\pi\epsilon_0(\beta\gamma)^3Mc^3]$. To lowest order in \bar{X}/ρ , the added path length due to bends can be accounted for in Eq. (1) by the substitution

$$\delta s_n \rightarrow \delta s_n + \sum_{m=1}^{m_b} \frac{L_{bm}}{\rho_m} \bar{X}_i(s_{bm}), \quad (4)$$

where L_{bm} , ρ_m , and s_{bm} are respectively the length, bend radius, and axial location of m_b bends between the induction cells. Since \bar{X}_i depends on β_{n+1}^i directly through $\Delta p/p$ and γ_i , and indirectly through σ_0 and I_b , Eq. (1) becomes a transcendental equation for β_{n+1}^i and must be solved iteratively.

To calculate the full waveforms for acceleration and longitudinal-control, the modified Kim-Smith method is first used to generate waveforms for acceleration and compression only, ignoring the longitudinal component of the beam space-charge field. CIRCE is then run using these fields but with the longitudinal space-charge field artificially turned off, mimicking perfect longitudinal control. Finally, the beam current profile from this run is used to calculate the optimal ear field in each acceleration gap.

3 RESULTS

A large number of CIRCE runs have been carried out to study the effects of using higher-voltage cells in the LLNL small recirculator. This exploratory work uses simple acceleration schedules and a somewhat idealized lattice, ignoring fringe fields and errors, and employing sector bends instead of the more complicated ‘‘flat-plate’’ bends actually built. Nominal parameters of the small-recirculator are given in Table 1, and a detailed description of the lattice is found in Ref. [4]. With the nominal low-voltage pulsers, induction cells are required in thirty-four of the forty half-lattice periods. Three HLPs without acceleration are needed to insert the beam into the ring and to extract it, and a three-HLP extraction section is planned halfway around the ring. For this nominal case, the specified four-to-one reduction of the beam duration is obtained by imposing a velocity tilt as rapidly as possible, consistent with a maximum pulser voltage of 500V. The mid-point beam energy is taken to increase linearly with s except in the insertion/extraction sections, and the beam duration is specified so the first thirteen waveforms on the first lap are approximately triangular, with small deviations that account for the transverse space-charge field, and the remaining ones are nearly flat-topped.

After the final lap, centroid displacement X at the ends is about ± 0.3 cm, which is in fair agreement with the analytic estimate of Eq. (3). However, the plot in Fig. 1 of beam-head displacement for this case during the final lap shows substantial betatron oscillation, and the beam tail shows a similar betatron amplitude. This betatron motion arises because each pulse with a head-to-tail voltage increase ΔV causes an abrupt change in the momentum tilt $\Delta p/p$ without significantly changing X . From Eq. (3), we expect the centroid to be mismatched by an amount $\delta X \sim \delta(\Delta p/p)$, and a simple calculation using Eq. (2)

Table 1 Parameters of the LLNL small recirculator

beam parameters		
ion charge state	q	1
ion mass	M	39 amu
beam current	I_b	2 \rightarrow 8 mA
kinetic energy	$(\gamma_0 - 1)Mc^2$	80 \rightarrow 320 MeV
duration	Δt	4 \rightarrow 1 μ s
lattice parameters		
circumference	s_{\max}	14.4 m
half-period	L	36 cm
pipe radius	R	3.5 cm

shows that

$$\delta \left(\frac{\Delta p}{p} \right) \approx \frac{qe\Delta V}{2\bar{\gamma}_{mid}\bar{\beta}_{mid}^2 Mc^2}, \quad (5)$$

where $\bar{\beta}_{mid}$ is the average of β_{mid} before and after the cell and $\bar{\gamma}_{mid}$ is the corresponding Lorentz factor. The mismatches introduced in successive cells should add in a Markovian sense because the betatron wavelength of centroid motion is typically uncorrelated with the cell spacing. Therefore, if N pulses are used to give a specified energy increase and velocity tilt, so that $\Delta V \sim N^{-1}$, we expect the accumulated betatron amplitude to have the approximate scaling

$$\delta X \sim N^{\frac{1}{2}} \Delta V \sim N^{-\frac{1}{2}}. \quad (6)$$

3.1 Effects of pulser number

Comparing cases with from five to thirty-four cells per lap but with the same acceleration schedule, we find that the peak betatron amplitude at the beam ends approximately doubles going from thirty-four to eighteen cells, but then drops significantly for the ten-cell case, as seen in Fig. 1. This improvement results from the periodic spacing of cells that is possible in the ten-cell case. The two insertion/extraction sections prevent equal cell spacing in the lattices with eighteen and thirty-four cells, but when cells are added to these sections to make periodic lattices with respectively twenty and forty cells, the betatron motion at the beam ends becomes very similar to that for the ten-cell case. For the eight-cell and five-cell cases, the betatron oscillations are progressively worse due to the larger ΔV in the triangular pulses, effectively prohibiting the use of triangular waveforms in these lattices.

3.2 Effects of pulser waveforms

The mismatch of the beam ends caused by head-to-tail voltage variation can be reduced by using a smaller ΔV in a correspondingly larger number of induction cells. For the same overall compression, each lattice studied shows a reduction in beam-end betatron motion when a schedule with triangular pulses is replaced by one using a larger number of trapezoidal pulses. The minimum betatron amplitude is seen when trapezoidal pulses are used on all

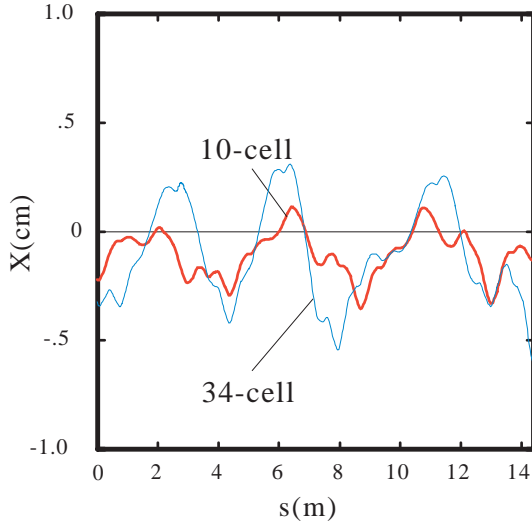


Fig. 1 Beam-head centroid displacement during the final lap in lattices with ten and thirty-four cells, with velocity tilt imposed rapidly during the first lap.

fifteen laps, as illustrated in Fig. 2. In lattices with regular cell spacing, we find that betatron motion introduced at the beam ends by a voltage tilt becomes negligible when $\Delta p/p$ changes in a cell by less than about 0.1%. Using Eq. (5), this criterion can be written to lowest order in β_{mid}^2 as

$$\frac{qe\Delta V}{\frac{1}{2}\bar{\beta}_{mid}^2 M c^2} \lesssim 0.004, \quad (7)$$

where $\frac{1}{2}\bar{\beta}_{mid}^2 M c^2$ is the beam kinetic energy in the non-relativistic limit. Nonperiodic cell spacing introduces an additional mismatch, leading to the fluctuations seen in Fig. 2 for thirty-four cells.

Another result of applying a reduced ΔV in more cells is that the maximum displacements of the beam head and tail increase. As the velocity tilt is applied more gradually, $\Delta p/p$ reaches its maximum of about 3% later in the acceleration sequence, and since σ_0 decreases roughly like β^{-1} for magnetic focusing, the average displacement at this point is larger, as seen from Eq. (3). Optimizing the acceleration schedule for a recirculator entails balancing this increased displacement against the reduced betatron amplitude found with a more gradual introduction of velocity tilt. The velocity tilt should therefore be introduced the as rapidly as possible without initiating betatron oscillations at the beam ends, as determined by Eq. (7).

3.3 Emittance growth

The 3-D particle-in-cell code WARP3d [3] has been used to corroborate selected CIRCE results and to study emittance growth. In these comparisons, WARP3d used acceleration and ear fields generated by CIRCE and the same idealized lattice elements. As in CIRCE runs, WARP3d simulations using trapezoidal waveforms on all fifteen laps show substantially higher betatron amplitude in cases with thirty-four cells per lap than with ten. However, the amplitude is noticeably higher in both cases than in the corresponding CIRCE runs, evidently due to a poorer initial

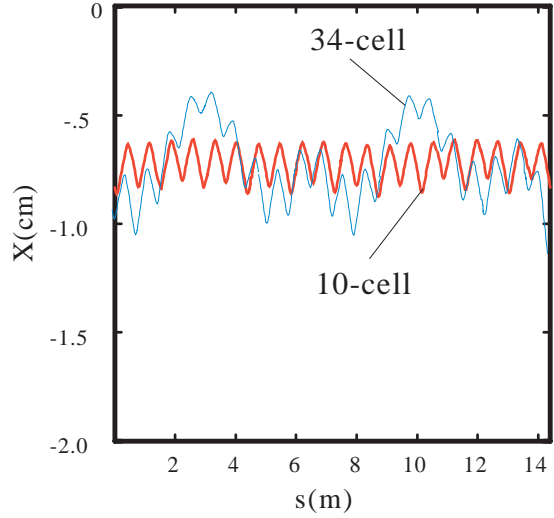


Fig. 2 Beam-head centroid displacement during the final lap in lattices with ten and thirty-four cells, with velocity tilt imposed gradually during all fifteen laps.

match. The particle simulations with thirty-four cells also show a larger and denser ‘‘halo’’ of unconfined particles near the ends than the ten-cell simulations, resulting in a higher x -emittance near the ends. For both cases, the normalized emittance near the mid-point increases about 68% during the fifteen laps, but the increase is greater than 165% at two maxima near the ends for thirty-four cells, whereas no emittance growth above the mid-point value is seen the ten-cell case. The enhanced loss of ions near the beam ends in the thirty-four cell case appears to be another effect of nonperiodic cell spacing, since it is not seen in WARP3d runs in lattices with twenty or forty cells per lap.

4 CONCLUSIONS

The CIRCE and WARP3d simulations here indicate that beam in the LLNL small recirculator can be accelerated and compressed using as few as five acceleration cells per lap, provided that the velocity tilt is added gradually enough to avoid initiating betatron oscillations near the beam ends. A layout having ten uniformly spaced cells, with trapezoidal pulses used on perhaps the first five of the fifteen laps, appears optimum. This schedule produces acceptably small betatron oscillations at the beam ends, while keeping the centroid displacement less than 0.7 cm.

5 REFERENCES

- [1] W. M. Sharp, J. J. Barnard, D. P. Grote, S. M. Lund, and S. S. Yu, ‘‘Envelope Model of Beam Transport in ILSE,’’ in *Proc. of the 1993 Computational Accelerator Physics Conference*, 22-26 February 1993, Pleasanton, CA, p. 540-548.
- [2] C. H. Kim and L. Smith, ‘‘A Design Procedure for Acceleration and Bunching in Ion Induction Linac,’’ Lawrence Berkeley Laboratory Rpt. LBL-19137 (1985).
- [3] D. P. Grote, A. Friedman, I. Haber, and S. S. Yu, *Fusion Engineering and Design* **32-33**, 193 (1996).
- [4] J. J. Barnard, *et al.*, *Fusion Engineering and Design* **32-33**, 247-258 (1996).